

SANDIA REPORT

SAND97-2772 • UC-705

Unlimited Release

Printed November 1997

Aspects of the Micro-Scale Acoustics of a Fluid Loaded Flexural Plate Wave Sensor

Jeffrey L. Dohner

Prepared by
Sandia National Laboratories
Albuquerque, New Mexico 87185 and Livermore, California 94550

Sandia is a multiprogram laboratory operated by Sandia Corporation, a Lockheed Martin Company, for the United States Department of Energy under Contract DE-AC04-94AL85000.

Approved for public release; further dissemination unlimited.



Sandia National Laboratories

Issued by Sandia National Laboratories, operated for the United States Department of Energy by Sandia Corporation.

NOTICE: This report was prepared as an account of work sponsored by an agency of the United States Government. Neither the United States Government nor any agency thereof, nor any of their employees, nor any of their contractors, subcontractors, or their employees, makes any warranty, express or implied, or assumes any legal liability or responsibility for the accuracy, completeness, or usefulness of any information, apparatus, product, or process disclosed, or represents that its use would not infringe privately owned rights. Reference herein to any specific commercial product, process, or service by trade name, trademark, manufacturer, or otherwise, does not necessarily constitute or imply its endorsement, recommendation, or favoring by the United States Government, any agency thereof or any of their contractors or subcontractors. The views and opinions expressed herein do not necessarily state or reflect those of the United States Government, any agency thereof or any of their contractors.

Printed in the United States of America. This report has been reproduced directly from the best available copy.

Available to DOE and DOE contractors from
Office of Scientific and Technical Information
PO Box 62
Oak Ridge, TN 37831

Prices available from (615) 576-8401, FTS 626-8401

Available to the public from
National Technical Information Service
US Department of Commerce
5285 Port Royal Rd
Springfield, VA 22161

NTIS price codes
Printed copy: A08
Microfiche copy: A01

Aspects of the Micro-Scale Acoustics of a Fluid Loaded Flexural Plate Wave Sensor

Jeffrey L. Dohner
Structural Dynamics Department
Sandia National Laboratories
P.O.Box 5800
Albuquerque, NM 87185-0439

Abstract

In this report, a study of wave propagation and damping in a fluid loaded Flexural Plate Wave (FPW) sensor is presented. Previous to this study, it was believed that supersonic radiation was the dominate mechanism of loss in FPW devices. However, because no previous theory had been developed to explain finite length effects, this belief was never challenged. In this paper, it will be shown that the dominate mechanism of damping is not only due to supersonic radiation, but is also due to a fluid/structure resonance arising from finite length effects.

The two-dimensional equations of motion for a single port FPW sensor plate are derived and coupled to the equations of motion for a viscous Newtonian fluid. These coupled equations are solved by using a wave number transform approach. This approach captures dynamics due to source terms at infinity. The resulting solution is comprised of terms derived by Wenzel, plus additional terms representing diffracted wave dynamics. The displacement field above the plate is then determined by using the Helmholtz integral equation.

Intentionally Left Blank

Acknowledgment

I would like to extend my special thanks to Dr. Steven J. Martin of Department 1315. Without his special insight into this problem, the solution would have never been found. I would also like to thank Michael Butler, Kurt Schubert, and Terry Henricks for their insight and understanding in the critical stages of this research.

Intentionally Left Blank

Contents

Acknowledgment	v
Notation	viii

Aspects of the Micro-Scale Acoustics of a Fluid Loaded Flexural Plate Wave Sensor

1. Introduction.....	1
2. Derivation of Equations of Motion.....	1
3. Solution of the Equations of Motion.....	5
4. Numerical Results.....	9
5. Conclusions.....	13
6. References.....	13
7. Appendix.....	14

Figures

Figure 1. An illustration of a single port flexural plate wave sensor.	2
Figure 2. A two dimensional approximation of the single port sensor.	2
Figure 3: A differential element of the plate of the single port sensor.	3
Figure 4: Contour integration used to calculate $\tilde{I}_1(n, x)$	6
Figure 5. Relative contribution of response due to Wenzel's term and due to edge diffraction.	10
Figure 6: Calculated impedance of fluid loaded and unload sensor for sub-sonic waves in the plate.	10
Figure 7: Calculated impedance of fluid loaded and unload sensor for sonic waves in the plate.	11
Figure 8: Calculated impedance of fluid loaded and unload sensor for super-sonic waves in the plate.	11
Figure 9. Particle displacements in the loading fluid for sub-sonic wave propagation in the plate relative to the diffracted surface wave.	12
Figure 10. Particle displacements in the loading fluid for sonic wave propagation in the plate relative to the diffracted surface wave.	12
Figure 11. Particle displacements in the loading fluid for super-sonic wave propagation in the plate relative to the diffracted surface wave.	12

Tables

Table 1: Flexural plate wave material, electrical and geometric properties. 9

Notation

h - thickness of the plate	D - flexural rigidity
L_x - width of the plate	$j = \sqrt{-1}$
E - Young's modulus of plate material	ω - circular frequency
ν - Poisson's ratio of plate material	$\tilde{\phi}$ - dilatational potential
ρ_p - density of plate material	ψ - shear potential
T - tension in the plate	k_l - dilatational wave number
$u_x(x), u_y(x)$ - displacement of the plate	k_s - shear wave number
i - current in wires	Φ - wave number transform of dilatational potential
B - magnetic field	Ψ - wave number transform of shear potential
B - bulk modulus of fluid	γ - wave number transform variable
μ_o - shear viscosity of fluid	$q = \sqrt{k_l^2 - \gamma^2}, s = \sqrt{k_s^2 - \gamma^2}$
μ_{v_o} - bulk viscosity of fluid	$r = j\gamma\frac{h}{2}$
ρ - density of fluid	c_p - speed of sound in the plate
V_x - shear force in plate	c_d - diffracted wave speed of sound in fluid
M_x - moment in plate	$x(\omega) = \int_{-\infty}^{\infty} x(t)e^{j\omega t} dt$ - temporal Fourier transform
τ_{xy} - shear stress in fluid	$X(\gamma) = \int_{-\infty}^{\infty} x(x)e^{-j\gamma x} dx$ - spatial Fourier transform
τ_{yy} - normal stress in fluid	
$\theta = \frac{\partial u_y}{\partial x}$ - rotation of plate	
u_{y_1} - first perturbation of displacement	
T_o, T_1 - first perturbation of tension	
M_{x_1} - first perturbation of moment	
τ_{xy_1}, τ_{yy_1} - first perturbations of stresses	

1. INTRODUCTION

In fluid loaded microelectromechanical sensors, damping occurs due to energy losses in the structure and/or due to energy losses into the fluid. In Flexural Plate Wave (FPW) sensors [1], structural damping is usually small [2] and most energy is lost into the fluid. Losses into the fluid can be due to relaxation effects such as those caused by viscosity and heat transfer, or can be due to radiation effects such as those due to edge diffraction. In this paper, a study of damping losses due to viscous relaxation and radiation is presented.

Viscous relaxation occurs in a number of different processes. Two well studied processes are small amplitude fluid motion around a structure and squeeze [3]. The first process is similar to that which is found in a tuning fork. After excitation, the tuning fork slowly loses energy via irreversible viscous air motion around its prongs. This process can be represented by a lossy non-propagating wave solution. K. Kokubun, M. Hirata, et. al. [4] developed a “string of beads” model to represent this process, and H. Hosak, K. Itao, et. al. [2] used Kokubun’s model with a squeeze model to model the dynamics of a micro-beam. Other researchers have also expanded upon Kokubun’s work to calculate damping due to this process [5].

Another form of damping is radiation damping. Radiation damping is due to propagating waves which transport energy into an ambient fluid. Y.-H. Cho, B. M. Kwak, et. al. [6] developed a model for the fluid damping of a micro comb drive using a radiating shear wave solution. Their model was an improvement over a simpler Couette-type (non-wave) model. S. W. Wenzel [7, 8] developed a more complex wave model for viscous damping in a FPW sensor using a non-radiating solution. This solution can also be used to represent damping due to radiation. Wenzel assumed that plate dimensionality was infinite, and therefore, edge diffraction effects were neglected. In this paper, the Wenzel model will be extended to include these neglected effects. It will be shown that diffracted waves can have a catastrophic effect on sensor performance.

2. DERIVATION OF EQUATIONS OF MOTION

A single port, Lorentz actuated FPW sensor [8] is modeled. In Figure 1 the FPW sensor is illustrated. This sensor consists of a thin SiN plate/membrane with a serpentine layer of gold wire laid back and forth across its length. The SiN plate is supported by a Si base which produces a clamped boundary condition at its edges. The FPW sensor operates by exciting a predominate mode of the plate. Excitation of this mode is produced by a Lorentz force resulting from the interaction of a current, i , with a supplied magnetic field, B .

Assuming that the length of the SiN plate is long compared to its width and that the excited mode is comprised of waves with low wave numbers in the length direction, a two dimensional analysis is appropriate. Moreover, for high wave numbers in the width direction, a simply supported boundary condition can be assumed. In this paper, less than 7% error in the natural frequency of the excited mode occurs due to this assumption¹.

Using the above assumptions, the complex three dimensional Figure 1 system can be approximated by a less complex, two dimensional Figure 2 system. The dynamics of this two dimensional approximation can be solved for in closed form. Thus, it will supply greater insight into relevant physics.

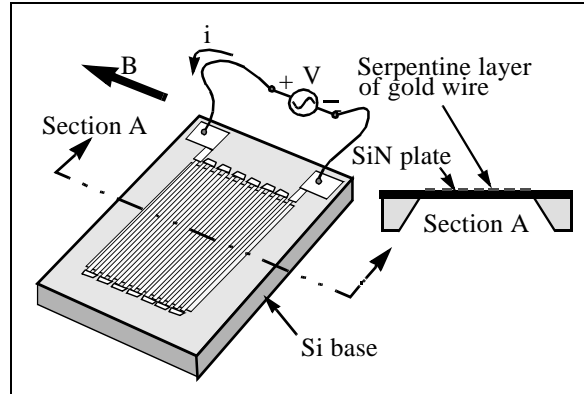


Figure 1. An illustration of a single port flexural plate wave sensor.

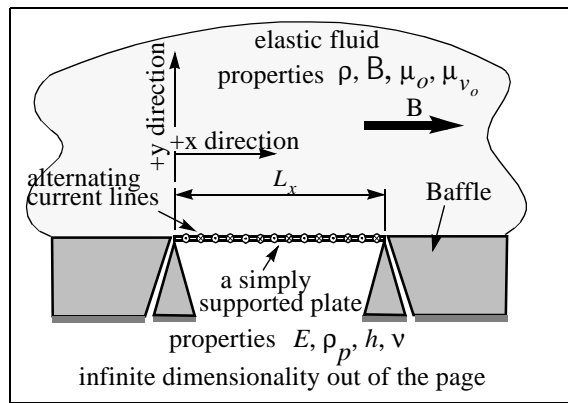


Figure 2. A two dimensional approximation of the single port sensor.

In the simplified system, the plate is h thick, is L_x long, and is comprised of a SiN linear elastic material with Elastic modulus, E , Poisons ratio, ν , and density, ρ_p . The plate contains an internal force per unit length, T . A differential element of the plate can move with x and y displacement, $u_x(x)$, and $u_y(x)$. Current lines run back and forth across the infinite width of the plate. Current, i , interacting with a supplied magnetic field, B , produces a Lorentz force excitation on the plate. Current is driven by a voltage per unit length, V . An semi-infinite linear Newtonian fluid with bulk modulus, B , shear viscosity, μ_o , bulk viscosity, μ_{v_o} , and density, ρ , loads the plate.

A differential element of the plate is shown in Figure 3. The shear force in the plate is V_x , the moment in the plate is M_x , the rotation of the plate is θ , the fluid shear stress on the

1. This assumption was validated by using a finite element analysis.

plate is τ_{xy} , the normal stress on the plate is τ_{yy} , and the tension in the plate is T . Summing forces in the y direction gives

$$\frac{\partial V_x}{\partial x} + T \frac{\partial \theta}{\partial x} + \theta \frac{\partial T}{\partial x} - \tau_{yy} = \rho_p h \frac{\partial^2 u_y}{\partial t^2} . \quad (1)$$

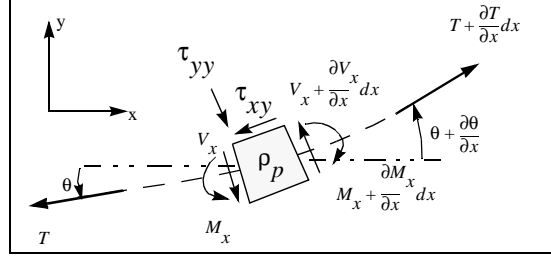


Figure 3. A differential element of the plate of the single port sensor.

Summing the moments gives

$$V_x = \frac{\partial M_x}{\partial x} - \frac{h}{2} \tau_{xy} . \quad (2)$$

Combining (1) and (2) and noting that $\theta = \frac{\partial u_y}{\partial x}$ gives a non-linear equation of motion for the plate

$$\frac{\partial^2 M_x}{\partial x^2} - \frac{h}{2} \frac{\partial \tau_{xy}}{\partial x} - \tau_{yy} + T \cdot \frac{\partial^2 u_y}{\partial x^2} + \frac{\partial u_y}{\partial x} \cdot \frac{\partial T}{\partial x} = \rho_p h \frac{\partial^2 u_y}{\partial t^2} . \quad (3)$$

The linearized equation of motion can be determined by perturbation analysis where $u_y = u_{y1} \varepsilon$, $T = T_o + T_1 \varepsilon$, $M_x = M_{x1} \varepsilon$, $\tau_{xy} = \tau_{xy1} \varepsilon$, $\tau_{yy} = \tau_{yy1} \varepsilon$, and ε is a small value.

Substituting these equations into (3) and collecting ε order terms gives

$$\frac{\partial^2 M_{x1}}{\partial x^2} + T_o \frac{\partial^2 u_{y1}}{\partial x^2} - \rho_p h \frac{\partial^2 u_{y1}}{\partial t^2} = \frac{h}{2} \frac{\partial \tau_{xy1}}{\partial x} + \tau_{yy1} . \quad (4)$$

Using classical analysis [9,10], the moment, M_{x1} , is related to the normal displacement as

$$M_{x1} = -D \frac{\partial^2 u_{y1}}{\partial x^2} \quad (5)$$

where $D = \frac{Eh^3}{12(1-\nu^2)}$. Substituting (4) into (5) and taking the temporal Fourier transform gives

$$\left(\frac{D}{\rho_p h} \frac{\partial^2}{\partial x^2} - \frac{T_o}{\rho_p h} \right) \cdot \frac{\partial^2 \tilde{u}_{y1}}{\partial x^2} - \omega^2 \frac{\partial^2 \tilde{u}_{y1}}{\partial t^2} = \frac{-1}{\rho_p h} \left(\tilde{\tau}_{yy1} + \frac{h}{2} \frac{\partial \tilde{\tau}_{xy1}}{\partial x} \right) , \quad (6)$$

where $\tilde{x} = \int_{-\infty}^{\infty} x e^{j\omega t} dt$, $j = \sqrt{-1}$, and ω is a circular frequency.

Equation 6 is the linear equation of motion of a plate driven by an external normal and shear stress. This equation was derived here to show the inclusion of the shear stress excitation τ_{xy} which is usually neglected in most plate analysis [9,10]. The normal stress can be expressed in terms of a stress due to the fluid and a stress due to the Lorentz force excitation as

$$\tilde{\tau}_{yy_1} = -iB \sum_{k=1}^{\infty} (-1)^{k-1} \delta\left(x - \frac{2k-1}{28}L_x\right) + \tilde{\tau}_{yy_1f} \quad (7)$$

where τ_{yy_1f} is the normal stress on the plate due to the fluid and $\delta(x)$ is a Dirac delta function.

Combining (7) with (6) and decomposing the result into in vacuo modes gives

$$a_m \left(\frac{\tilde{A}_m}{i} \right) = b_m - \frac{1}{\rho_p h} \int_0^{L_x} \frac{\tilde{g}(x)}{i} \sin\left(\frac{m\pi}{L_x}x\right) dx \quad (8)$$

where $a_m = \frac{L_x}{2}(\omega_m^2 - \omega^2)$, $\omega_m^2 = \left(\frac{D}{\rho_p h} \left(\frac{m\pi}{L_x}\right)^2 + \frac{T_o}{\rho_p h}\right) \left(\frac{m\pi}{L_x}\right)^2$, $\tilde{u}_{y_1} = \sum_{m=1}^{\infty} \tilde{A}_m \sin\left(\frac{m\pi}{L_x}x\right)$

$b_m = \frac{B}{\rho_p h} \sum_{k=1}^{\infty} -1^{k-1} \sin\left(m\pi \frac{(2k-1)}{28}\right)$, and $\tilde{g}(x) = \tilde{\tau}_{yy_1f} + \frac{h}{2} \frac{\partial \tilde{\tau}_{xy_1}}{\partial x}$. Equation 8 is a modal

representation of plate dynamics. In the following section, the function $\tilde{g}(x)$ will be represented in terms of these same modes.

Following Temkin [11], the linearized displacement of the fluid can be represented as

$$\tilde{u}_{x_1} \hat{i} + \tilde{u}_{y_1} \hat{j} = \nabla \tilde{\phi} + \nabla \times \tilde{\psi} \quad (9)$$

where \tilde{u}_{x_1} and \tilde{u}_{y_1} is the x and y displacement of a fluid particle, \hat{i} and \hat{j} are x and y direction unit vectors, and $\tilde{\phi}$ and $\tilde{\psi}$ are potential functions where

$$\left(\nabla^2 + k_l^2\right)\tilde{\phi} = 0, \quad \left(\nabla^2 + k_s^2\right)\tilde{\psi} = 0, \quad (10,11)$$

$$k_l^2 = \frac{\omega^2/c_o^2}{4v'_o} = \frac{\omega^2}{c_l^2}, \quad k_s^2 = \frac{\omega^2}{-j\omega v_o} = \frac{\omega^2}{c_s^2}, \quad (12,13)$$

$c_o^2 = \frac{B}{\rho}$ is the acoustic sound speed, $v'_o = \frac{1}{\rho}(\mu_o + \frac{3}{4}\mu_{v_o})$, and $v_o = \frac{\mu_o}{\rho}$ is the specific viscosity. In air, Temkin used the work of Greenspan [12], to approximate the bulk viscosity of air as $\mu_{v_o} \approx 0.65\mu_o$. Using the fact that $c_l^2 = \frac{\lambda + 2\mu}{\rho}$ and that $c_s^2 = \frac{\mu}{\rho}$ [13], $\mu = -j\omega\mu_o$ and $\lambda = B - j\omega(\mu_{v_o} - \frac{2}{3}\mu_o)$.

Equations 9,10,11 are the equations of motion for the fluid. These equation are coupled to the equations of motion of the plate by the stress displacement relations

$$\tau_{yy_1} = (\lambda + 2\mu) \left\{ \frac{\partial \tilde{u}_{y_1}}{\partial y} + \frac{\partial \tilde{u}_{x_1}}{\partial x} \right\} - 2\mu \frac{\partial \tilde{u}_{x_1}}{\partial x}, \quad (14)$$

$$\tau_{xy_1} = 2\mu \left\{ \frac{\partial \tilde{u}_{x_1}}{\partial y} + \frac{\partial \tilde{u}_{y_1}}{\partial x} \right\}, \quad (15)$$

and the potential displacement relations

$$\epsilon_{x_1} = \frac{\partial \tilde{\phi}}{\partial x} + \frac{\partial \tilde{\psi}}{\partial y}, \quad \epsilon_{y_1} = \frac{\partial \tilde{\phi}}{\partial y} - \frac{\partial \tilde{\psi}}{\partial x}, \quad (16,17)$$

evaluated at $y = 0$.

3. SOLUTION OF THE EQUATIONS OF MOTION

The equations of motion (6, 9,10,11) are solved by using a wave number transform approach.

3.1 Solution on the Surface

By definition, the wave number transform of ϕ is

$$\tilde{\Phi}(\gamma) = \int_{-\infty}^{\infty} \tilde{\phi}(x) e^{-j\gamma x} dx. \quad (18)$$

In the wave number domain, the solution to equations 10,11 can be written as

$$\tilde{\Phi} = \mathbf{A} e^{jqy} \text{ and } \tilde{\Psi} = \mathbf{B} e^{jsy}, \quad (19,20)$$

where $\Psi(\gamma)$ is the wave number transform of $\psi(x)$, $q = \sqrt{k_l^2 - \gamma^2}$ and $s = \sqrt{k_s^2 - \gamma^2}$. Following the derivation by Wenzel [7], taking the transform of equations 3c,d, making the assumption that $\tilde{u}_x(x, y = 0) \equiv -\frac{h}{2} \frac{\partial \tilde{u}_y}{\partial x}(x, y = 0)$ ¹ and solving for A and B gives

$$\mathbf{A} = \frac{js + j\gamma r}{\gamma^2 + qs} \text{ and } \mathbf{B} = \frac{jqr - j\gamma}{\gamma^2 + qs} \quad (21,22)$$

where $r = -j\gamma \frac{h}{2}$. Substituting equations 21 and 22 into equations 19 and 20, the result

1. This assumption comes from the derivation of flexural wave motion in a unloaded plate[10]. For light fluids this assumption is satisfactory, however for heavy fluids its validity becomes questionable. Here it is assumed that the fluid is air.

into the wave number transform of equations 16 and 17, that result into equation 14 and 15, that result into the wave number transform for the expression for $g(\tilde{x})$, simplifying and neglecting small terms gives

$$\frac{\tilde{G}(\gamma)}{\tilde{U}_y(\gamma, y=0)} = j\omega^2 \rho \frac{s}{\gamma^2 + sq} \quad (23)$$

where $\tilde{G}(\gamma)$ is the wave number transform of $\tilde{g}(x)$ and $\tilde{U}_y(\gamma)$ is the wave number transform of $\tilde{u}_y(x)$. Since $\tilde{u}_y(x, y=0)$ can be expressed in terms of the in vacuo modes of the plate and the wave number transform is a linear operator, $\tilde{U}_y(\gamma, y=0)$ can be expressed in terms of the wave number transform of the in vacuo modes of the plate. Representing $\tilde{U}_y(\gamma, y=0)$ in terms of in vacuo modes, solving for $\tilde{G}(\gamma)$ and inverse transforming gives

$$\tilde{g}(x) = -j\frac{\omega^2 \rho}{2\pi} \sum_{n=1}^{\infty} \tilde{A}_n \left[\tilde{I}_1(n, x) - (-1)^n \tilde{I}_1(n, x - L_x) \right], \quad (24)$$

$$\text{where } \tilde{I}_1(n, x) = \int_{-\infty}^{\infty} \frac{\frac{n\pi}{L_x} \sqrt{k_s^2 - \gamma^2} e^{-j\gamma x}}{\left(\left(\frac{n\pi}{L_x} \right)^2 - \gamma^2 \right) \left(\gamma^2 + \sqrt{k_s^2 - \gamma^2} \sqrt{k_l^2 - \gamma^2} \right)} d\gamma.$$

$\tilde{I}_1(n, x)$ can be solved by using a contour integration. The poles of the integrand of $\tilde{I}_1(n, x)$

are $\gamma_1 = \frac{n\pi}{L_x}$, $\gamma_2 = \frac{n\pi}{L_x}$, $\gamma_3 = -\sqrt{\frac{k_s^2 k_l^2}{k_s^2 + k_l^2}}$, and $\gamma_4 = \sqrt{\frac{k_s^2 k_l^2}{k_s^2 + k_l^2}}$, and the branch integrations

are shown in Figure 4. The integral, $\tilde{I}_1(n, x)$, can be determined from a contour integration

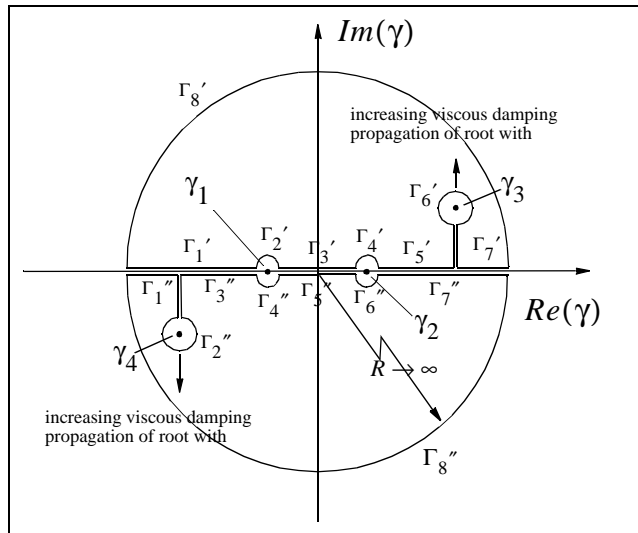


Figure 4. Contour integration used to calculate $\tilde{I}_1(n, x)$

over the upper or lower half of the γ plane. The use of the upper or lower half is depen-

dent upon the convergence of Γ_8' and Γ_8'' branches. Computing the integral of the $\tilde{I}_1(n, x)$ integrand over the Γ_8' branch, letting $\gamma = \lim_{R \rightarrow \infty} R e^{i\theta}$, and noting that

$$\lim_{R \rightarrow \infty} (R^2 e^{i2\theta} + \sqrt{k_s^2 - R^2 e^{i2\theta}} \sqrt{k_l^2 - R^2 e^{i2\theta}}) = \frac{k_s^2 + k_l^2}{2} \text{ gives}$$

$$\lim_{R \rightarrow \infty} \int_0^\pi \frac{\frac{n\pi}{L_x} \sqrt{k_s^2 - R^2 e^{i2\theta}} e^{-jxR \cos \theta} e^{xR \sin \theta}}{\left(\left(\frac{n\pi}{L_x} \right)^2 - R^2 e^{i2\theta} \right) \left(R^2 e^{i2\theta} + \sqrt{k_s^2 - R^2 e^{i2\theta}} \sqrt{k_l^2 - R^2 e^{i2\theta}} \right)} R i e^{i\theta} d\theta \rightarrow \begin{cases} \infty & \text{for } x > 0 \\ 0 & \text{for } x < 0 \end{cases}$$

Computing the integral over the Γ_8'' branch gives

$$\lim_{R \rightarrow \infty} \int_\pi^{2\pi} \frac{\frac{n\pi}{L_x} \sqrt{k_s^2 - R^2 e^{i2\theta}} e^{-jxR \cos \theta} e^{xR \sin \theta}}{\left(\left(\frac{n\pi}{L_x} \right)^2 - R^2 e^{i2\theta} \right) \left(R^2 e^{i2\theta} + \sqrt{k_s^2 - R^2 e^{i2\theta}} \sqrt{k_l^2 - R^2 e^{i2\theta}} \right)} R i e^{i\theta} d\theta \rightarrow \begin{cases} 0 & \text{for } x > 0 \\ \infty & \text{for } x < 0 \end{cases}.$$

Therefore, the lower set of branches can be used to evaluate $\tilde{I}_1(n, x)$ for $x > 0$ and the upper set of branches can be used to evaluate $\tilde{I}_1(n, x)$ for $x < 0$. The integration around other branches is calculated using standard techniques [14]. Substituting the result for $\tilde{I}_1(n, x)$ into (24) gives

$$\tilde{g}(x) = \sum_{n=1}^{\infty} \tilde{A}_n \left\{ \begin{array}{l} C_1(n) \sin\left(\frac{n\pi}{L_x} x\right) \text{ for } 0 < x < L_x \\ 0 \text{ otherwise} \end{array} \right\} + \left\{ \begin{array}{l} C_2(n) e^{-j \frac{\sqrt{k_s^2 k_l^2}}{\sqrt{k_s^2 + k_l^2}} x} \text{ for } x > 0 \\ C_2(n) e^{j \frac{\sqrt{k_s^2 k_l^2}}{\sqrt{k_s^2 + k_l^2}} x} \text{ for } x < 0 \\ -(-1)^n C_2(n) e^{-j \frac{\sqrt{k_s^2 k_l^2}}{\sqrt{k_s^2 + k_l^2}} (x - L_x)} \text{ for } x > L_x \\ -(-1)^n C_2(n) e^{j \frac{\sqrt{k_s^2 k_l^2}}{\sqrt{k_s^2 + k_l^2}} (x - L_x)} \text{ for } x < L_x \end{array} \right\} \quad (25)$$

where

$$C_1(n) = \frac{j\omega^2 \rho \sqrt{k_s^2 - \left(\frac{n\pi}{L_x}\right)^2}}{\left(\frac{n\pi}{L_x}\right)^2 - \sqrt{k_l^2 - \left(\frac{n\pi}{L_x}\right)^2} \sqrt{k_s^2 - \left(\frac{n\pi}{L_x}\right)^2}} \text{ and } C_2(n) = \frac{-\omega^2 \rho \frac{n\pi}{L_x} \frac{k_s^2}{\sqrt{k_s^2 + k_l^2}}}{\left(\frac{n\pi}{L_x}\right)^2 - \frac{k_s^2 k_l^2}{k_s^2 + k_l^2} \left(k_s^2 + k_l^2\right) \sqrt{\frac{k_s^2 + k_l^2}{k_s^2 k_l^2}}}.$$

The bracketed expression in (25) is the solution for the force on the plate due to the excitation of the n^{th} in vacuo mode. Notice that the first term in brackets is the result of Wenzel. The second set of terms in brackets are due to edge diffraction. Substituting (25) into (8) gives

$$a_m\left(\frac{\tilde{A}_m}{i}\right) = b_m + \sum_{n=1}^{\infty} c_{mn}\left(\frac{\tilde{A}_n}{i}\right) \quad (26)$$

where

$$c_{mn} = -\frac{1}{\rho_p h} \left\{ C_1(n) \frac{L_x}{2} \delta_{mn} - C_2(n) \frac{\frac{m\pi}{L_x}}{\left(\frac{m\pi}{L_x}\right)^2 - \frac{k_s^2 k_l^2}{k_s^2 + k_l^2}} \left[1 + (-1)^{m+n} - ((-1)^n + (-1)^m) e^{-j \frac{k_s^2 k_l^2}{k_s^2 + k_l^2} L_x} \right] \right\} \quad (27)$$

A matrix solution can be used to solve (26) for \tilde{A}_m where $n = 1, 2, 3 \dots$. This solution can then be used to solve for the impedance of the electrical system,

$$\frac{V}{i} = R - j\omega B \sum_{l=1}^{\infty} \sum_{m=1}^{\infty} \left(\frac{\tilde{A}_m}{i}\right) \sin\left(\frac{2l-1}{28} L_x\right) (-1)^{l-1} \quad (28)$$

3.2 Solution in the Domain

In the above subsection a wave number transform method was used to determine a closed form solution for $\tilde{g}(x)$ on the surface of the domain. If this same transform method were used to determine the solution in the domain, a branch cut would have to be made in Figure 4 which would require the numerical evaluation of a difficult integral. This difficulty can be avoided by the evaluation of potential functions on the surface of the domain, the use of the two-space Helmholtz integral equation, and the use of (9).

Using the method described in subsection 3.3, $\tilde{\phi}(x, y = 0)$, $\psi(x, y = 0)$, $\frac{\partial}{\partial y} \tilde{\phi}(x, y = 0)$, and

$\frac{\partial}{\partial y} \psi(x, y = 0)$ can be determined. These functions are given in the Appendix. The two-space

Helmholtz integral equation can then be used to determine $\tilde{\phi}(x, y)$ and $\psi(x, y)$. For $\tilde{\phi}(x, y)$, Helmholtz is written as

$$\tilde{\phi}(x, y) = \oint_{\Gamma} \left\{ G(k_p, x, y | x_o, y_o) \frac{\partial}{\partial y} \tilde{\phi}(x, y = 0) - \frac{\partial}{\partial y} G(k_p, x, y | x_o, y_o) \tilde{\phi}(x, y = 0) \right\} d\Gamma \quad (29)$$

where $G(k_p, x, y | x_o, y_o) = -\frac{j}{4} H_0^1(k_l R)$, $R = \sqrt{(x-x_o)^2 + (y-y_o)^2}$ and where Γ represents a contour extending along the surface of the plate, out to infinity and back. Since the Sommerfeld radiation condition [15] is not satisfied in two space acoustics, (29) cannot be used to solve for sources at infinity. The effects of sources at infinity were included in the wave number transform solution. Equation (29) will only be used to map information

from the surface of the domain, into the domain. Since $\lim_{\epsilon \rightarrow \infty} H_o^1 \rightarrow 0$, this mapping is local.

For $\psi(x, y)$, Helmholtz is written as

$$\tilde{\psi}(x, y) = \oint_{\Gamma} \left\{ G(k_s, x, y | x_o, y_o) \frac{\partial}{\partial y} \tilde{\psi}(x, y = 0) - \frac{\partial}{\partial y} G(k_s, x, y | x_o, y_o) \tilde{\psi}(x, y = 0) \right\} d\Gamma, \quad (30)$$

where $G(k_s, x, y | x_o, y_o) = -\frac{j}{4} H_0^1(k_s R)$ and $R = \sqrt{(x - x_o)^2 + (y - y_o)^2}$. The functions $\frac{\partial}{\partial y} \tilde{\psi}(x, y)$ and $\frac{\partial}{\partial y} \tilde{\psi}(x, y)$ can be determined by taking the spatial derivatives of (29) and (30), and u_{x_1} and u_{u_1} can be determined from (9).

4. NUMERICAL RESULTS

In this section, the equations of motion will be solved for an air loaded SiN plate. The properties of the plate and air are given in Table 1. The tension in the plate was adjusted such that the excited mode always had a natural frequency of 0.406 Mhz. To study the mechanisms by which the plate loses energy to the fluid, the length of the plate was varied. As the length of the plate was varied, the sound speed of waves in the plate was altered by an associated variation in tension. Plate sound speeds were sub-sonic, super-sonic, or sonic to waves in the fluid. The major damping mechanism in the plate was that due to a resonance in both the fluid and the structure. This resonance occurred when the waves in the plate were sonic to diffracted waves in the fluid.

This resonance can be seen in (25). The first term in the outer brackets of this equation is the forced excitation response. Notice that the C_1 coefficient in front of the this term is Wenzel's expression for fluid loading. The second set of terms represent loading due to edge diffraction. These terms are proportional to C_2 . In Figure 5, the coefficients, C_1

Table 1
Flexural plate wave material, electrical and geometric properties

SiN properties	value	electrical properties	value
E	$0.27 \text{ N}/\mu\text{m}^2$	B	$7.78 \cdot 10^{-7} \text{ N}/(\text{A} \cdot \mu\text{m})$
ρ_p	$2.95 \cdot 10^{-21} \text{ kg} \cdot \text{m}/\mu\text{m}^4$	R	$7.87 \cdot 10^{-3} \Omega/(\mu\text{m})$
ν	0.24		
geometric properties	value	air properties	value
L_x	$2000 \mu\text{m}$	B	$2.14 \cdot 10^{-7} \text{ N}/\mu\text{m}^2$
h	$1 \mu\text{m}$	ρ	$1.77 \cdot 10^{-24} \text{ kg} \cdot \text{m}/\mu\text{m}^4$
		μ	$1.85 \cdot 10^{-11} \text{ kg}/\mu\text{m} \cdot \text{s}$

and C_2 , are evaluated versus c_p/c_d where c_p is the sound speed of a wave in the plate and

c_d is the sound speed of a diffracted wave with wave number $\sqrt{\frac{k_s^2 k_l^2}{k_s^2 + k_l^2}}$. Near the sonic con-

dition, edge diffraction dominates plate loading ($|C_2|$ is big). Above and below the sonic condition, both C_1 and C_2 are small. This represents the response of a resonance condi-

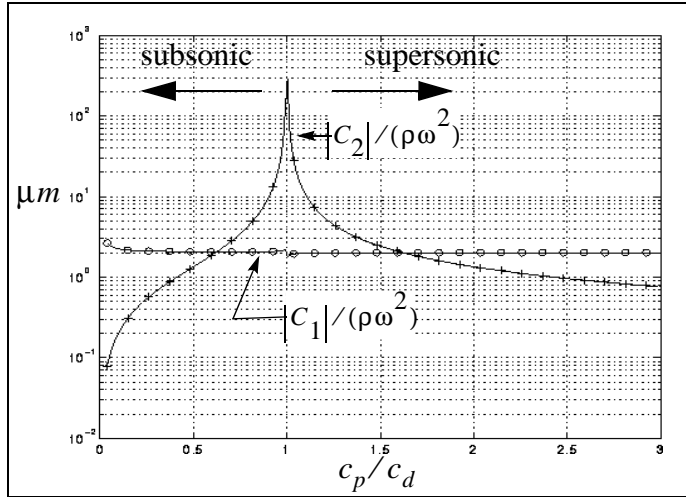


Figure 5. Relative contribution of response due to Wenzel's term and due to edge diffraction.

In Figures 6, 7, and 8 the impedance response of the fluid loaded FPW for sub-sonic, sonic, and super-sonic waves in the plate is shown. Also shown in Figures 6, 7, and 8 are the impedance

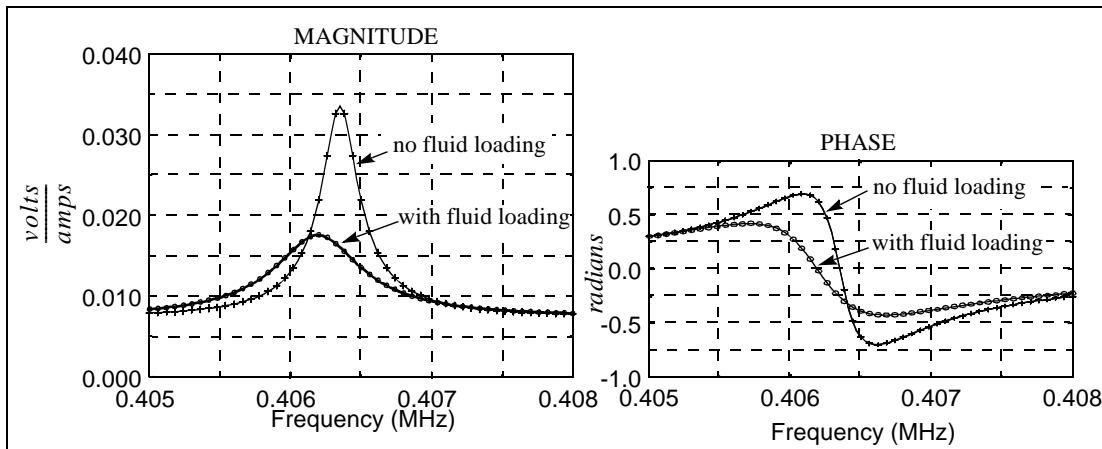


Figure 6. Calculated impedance of fluid loaded and unload sensor for sub-sonic waves in the plate. $c_p/c_d = 0.336$.

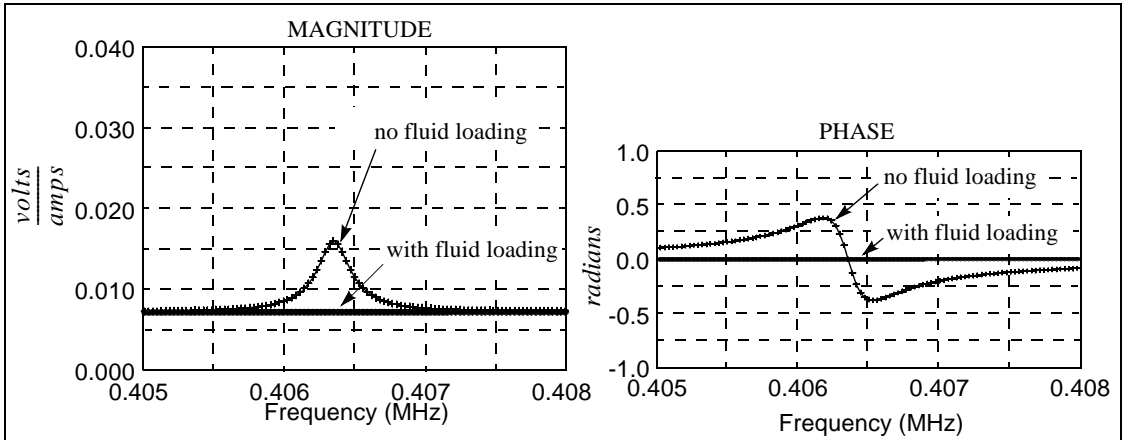


Figure 7. Calculated impedance of fluid loaded and unload sensor for sonic waves in the plate $c_p/c_d = 1.00$

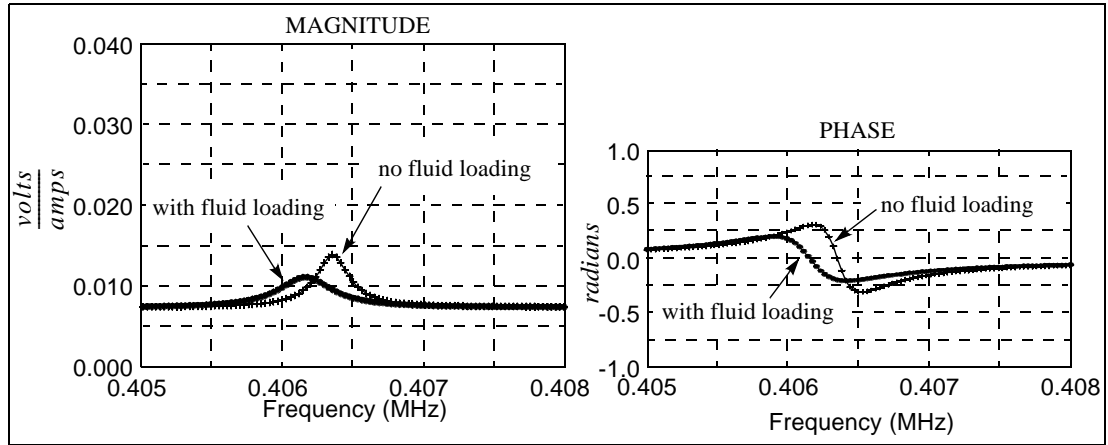


Figure 8. Calculated impedance of fluid loaded and unload FPW sensor for super-sonic waves in the plate. $c_p/c_d = 1.34$

responses of the FPW without fluid loading. If the viscosity of the fluid were zero in any condition, the fluid loaded and unloaded responses would be similar. Therefore, the dominate mechanism of damping into the fluid is not due to radiation but due to viscous relaxation. At fluid/structure resonance, this loss is the greatest.

The displacement field above the plate can be determined from (29) and (30). Figure 9,10, and 11 show the displacement in the fluid for sub-sonic, sonic, and super sonic conditions. Notice the ordinate changes between each plot.

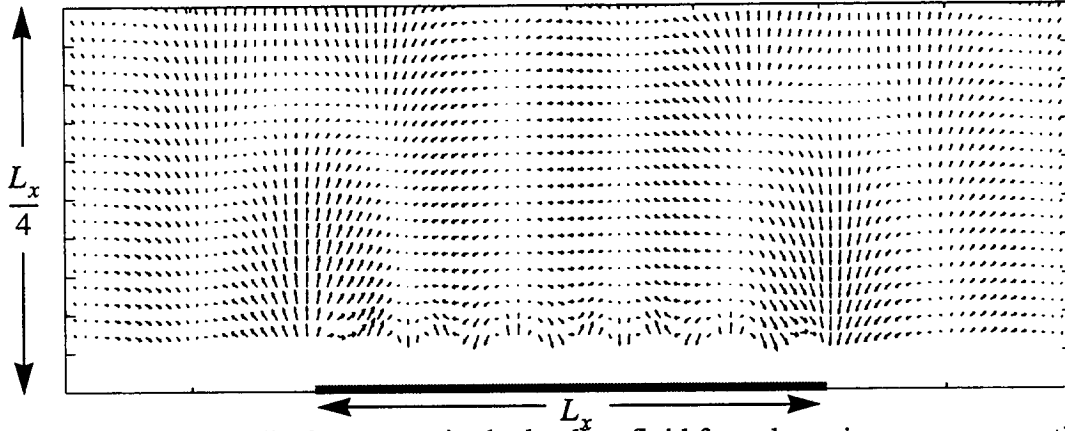


Figure 9. Particle displacements in the loading fluid for sub-sonic wave propagation in the plate relative to the diffracted surface wave. $c_p/c_d = 0.336$.

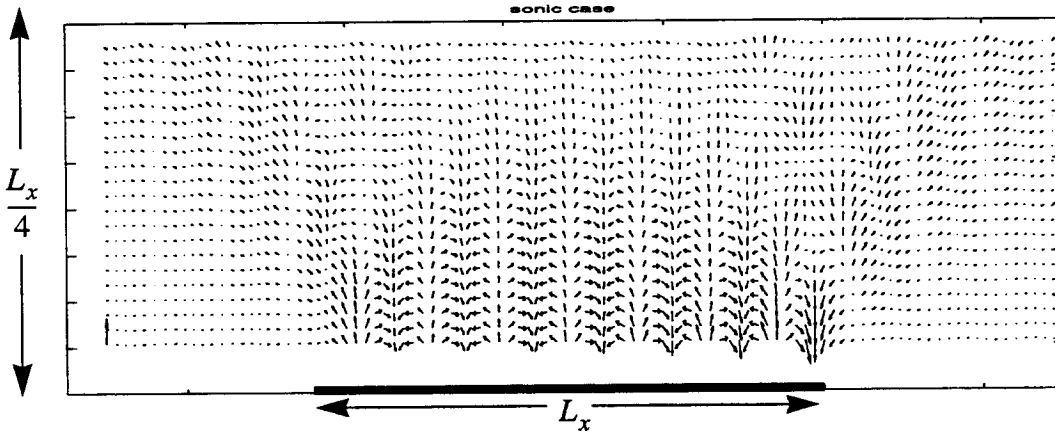


Figure 10. Particle displacements in the loading fluid for sonic wave propagation in the plate relative to the diffracted surface wave. $c_p/c_d = 1.00$.

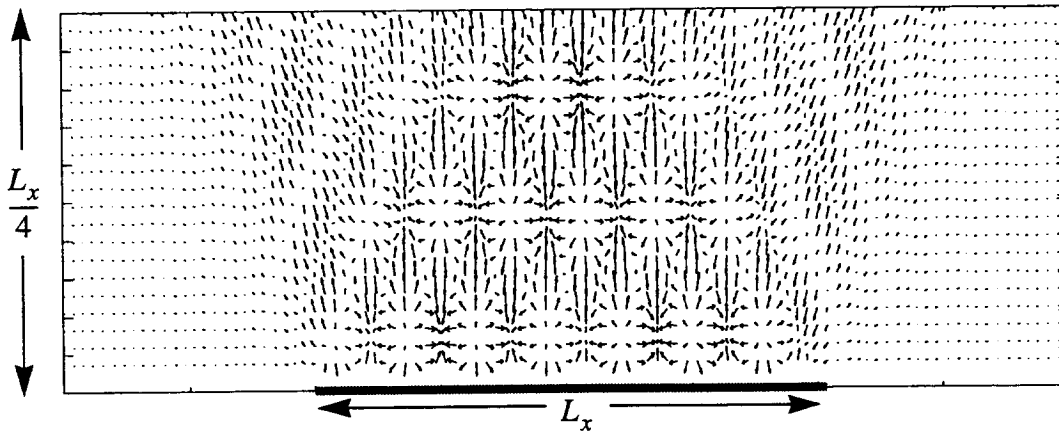


Figure 11. Particle displacements in the loading fluid for super-sonic wave propagation in the plate relative to the diffracted surface wave. $c_p/c_d = 1.34$.

5. CONCLUSIONS

In this paper, a new model representing the mechanisms of radiation and viscous relaxation in a fluid loaded Flexural Plate Wave (FPW) sensor was presented. From this model, it was determined that when the wave number of the FPW plate is close to the wave number of a diffracted surface wave, a fluid/structure resonance exists which produces substantial energy loss from the structure. This mechanism of viscous loss has not been cited in the previous literature. It is a new understanding of the limitations which bound the operation of FPW devices.

Previous to this, it was believed that supersonic radiation was the dominant mechanism of damping in these devices. Because no previous theory had been developed to explain finite length effects, this belief was never challenged. In this paper, it was determined that the major mechanism of loss into the fluid was not due to supersonic radiation, but due to a fluid/structure resonance.

6. REFERENCES

1. S. M. SZE 1994 *Semiconductor Sensors*. New York: John Wiley.
2. H. HOSAKA, K. ITAO and S. KURODA 1995 *Sensors and Actuators, A Physical* **A49**(1-2), 87-95. Damping characteristics of beam-shaped micro-oscillators.
3. M. K. ANDREWS and P. D. HARRIS 1995 *Sensors and Actuators, A Physical* **A49**(1-2), 103-108. Damping and gas viscosity measurements using a microstructure.
4. K. KOKUBUN, M. HIRATA, H. MURAKAMI, Y. TODA and M. ONO 1984 *Vacuum* **34**(8-9), 731-735. A bending and stretching mode crystal oscillator as a friction vacuum gauge.
5. Z. KADAR, A. BOSSCHE and J. MOLLINGER 1995 *Sensors and Actuators, A Physical* **A46-47**(1-3), 623-627. Design of a single-crystal silicon-based micromechanical resonator using finite element simulations.
6. Y.-H. CHO, B. M. KWAK, A. P. PISANO and R. T. HOWE 1993 *Proceedings of Micro Electro Mechanical Systems*, 93-98, IEEE: New York. Viscous energy dissipation in laterally oscillating planar microstructures: a theoretical and experimental study.
7. S. W. WENZEL 1982 Ph.D Thesis, Department of Electrical Engineering and Computer Sciences, University of California, Berkeley, CA. *Applications of Ultrasonic Lamb Waves*.
8. S. J. MARTIN, M. A. BUTLER, J. J. SPATES, W. K. SCHUBERT and M. A. MITCHELL 1997 *Proceedings of the 1997 IEEE International Frequency Control Symposium*, 20-30, IEEE: New York. Magnetically-excited flexural plate wave resonator.
9. K. F. GRAFF 1975 *Wave Motion in Elastic Solids*. Dover Publications: New York.

10. L. CREMER, M. HECKL and E. E. UNGAR 1988 *Structure-Borne Sound; Structural Vibrations and Sound Radiation at Audio Frequencies*. Springer-Verlag: New York.
11. S. TEMKIN 1981 *Elements of Acoustics*. John Wiley: New York.
12. M. GREENSPAN 1959 *Journal of the Acoustics Society of America* **32**(2), 70-73. Rotational relaxation in nitrogen, oxygen, and air.
13. J. D. ACHENBACK 1987 *Wave Propagation in Elastic Solids*. North-Holland: New York.
14. G. F. CARRIER, M. KROOK and C. E. PEARSON 1983 *Functions of a Complex Variable; Theory and Technique*. McGraw-Hill: New York.
15. M.C.JUNGER and D.FEIT 1986 *Sound, Structures, and Their Interaction*. The MIT Press: Cambridge.

APPENDIX

In this appendix expressions for $\tilde{\phi}(x, y = 0)$, $\Psi(x, y = 0)$, $\frac{\partial}{\partial y}\tilde{\phi}(x, y = 0)$, and $\frac{\partial}{\partial y}\tilde{\psi}(x, y = 0)$ are presented. These expressions were derived using a wave number transform approach.

$$\tilde{\psi}(x) = \sum_{n=1}^{\infty} \tilde{A}_n \left\{ \begin{array}{ll} C_3(n) \sin\left(\frac{n\pi}{L_x}x\right) & \text{for } 0 < x < L_x \\ 0 & \text{otherwise} \end{array} \right\} + \left\{ \begin{array}{ll} C_4(n)e^{-j\sqrt{\frac{k_s^2 k_l^2}{2^2 + k_l^2}}x} & \text{for } x > 0 \\ C_4(n)e^{j\sqrt{\frac{k_s^2 k_l^2}{2^2 + k_l^2}}x} & \text{for } x < 0 \\ -(-1)^n C_4(n)e^{-j\sqrt{\frac{k_s^2 k_l^2}{2^2 + k_l^2}}(x - L_x)} & \text{for } x > L_x \\ -(-1)^n C_4(n)e^{j\sqrt{\frac{k_s^2 k_l^2}{2^2 + k_l^2}}(x - L_x)} & \text{for } x < L_x \end{array} \right\}$$

$$\frac{\partial}{\partial y} \tilde{\phi}(x) = \sum_{n=1}^{\infty} \tilde{A}_n \left\{ \begin{array}{ll} C_5(n) \sin\left(\frac{n\pi}{L_x} x\right) & \text{for } 0 < x < L_x \\ 0 & \text{otherwise} \end{array} \right\} + \left\{ \begin{array}{ll} C_6(n) e^{-j \sqrt{\frac{k_s^2 k_l^2}{2^2 + k_l^2}} x} & \text{for } x > 0 \\ C_6(n) e^{j \sqrt{\frac{k_s^2 k_l^2}{2^2 + k_l^2}} x} & \text{for } x < 0 \\ -(-1)^n C_6(n) e^{-j \sqrt{\frac{k_s^2 k_l^2}{2^2 + k_l^2}} (x - L_x)} & \text{for } x > L_x \\ -(-1)^n C_6(n) e^{j \sqrt{\frac{k_s^2 k_l^2}{2^2 + k_l^2}} (x - L_x)} & \text{for } x < L_x \end{array} \right\}$$

$$\tilde{\Psi}(x) = \sum_{n=1}^{\infty} \tilde{A}_n \left\{ \begin{array}{ll} C_7(n) \cos\left(\frac{n\pi}{L_x} x\right) & \text{for } 0 < x < L_x \\ 0 & \text{otherwise} \end{array} \right\} + \left\{ \begin{array}{ll} C_8(n) e^{-j \sqrt{\frac{k_s^2 k_l^2}{2^2 + k_l^2}} x} & \text{for } x > 0 \\ -C_8(n) e^{j \sqrt{\frac{k_s^2 k_l^2}{2^2 + k_l^2}} x} & \text{for } x < 0 \\ -(-1)^n C_8(n) e^{-j \sqrt{\frac{k_s^2 k_l^2}{2^2 + k_l^2}} (x - L_x)} & \text{for } x > L_x \\ (-1)^n C_8(n) e^{j \sqrt{\frac{k_s^2 k_l^2}{2^2 + k_l^2}} (x - L_x)} & \text{for } x < L_x \end{array} \right\}$$

$$\frac{\partial}{\partial y} \tilde{\Psi}(x) = \sum_{n=1}^{\infty} \tilde{A}_n \left\{ \begin{array}{ll} C_9(n) \cos\left(\frac{n\pi}{L_x} x\right) & \text{for } 0 < x < L_x \\ 0 & \text{otherwise} \end{array} \right\} + \left\{ \begin{array}{ll} C_{10}(n) e^{-j \sqrt{\frac{k_s^2 k_l^2}{2^2 + k_l^2}} x} & \text{for } x > 0 \\ -C_{10}(n) e^{j \sqrt{\frac{k_s^2 k_l^2}{2^2 + k_l^2}} x} & \text{for } x < 0 \\ -(-1)^n C_{10}(n) e^{-j \sqrt{\frac{k_s^2 k_l^2}{2^2 + k_l^2}} (x - L_x)} & \text{for } x > L_x \\ (-1)^n C_{10}(n) e^{j \sqrt{\frac{k_s^2 k_l^2}{2^2 + k_l^2}} (x - L_x)} & \text{for } x < L_x \end{array} \right\}$$

where

$$C_3(n) = \frac{j \sqrt{k_s^2 - \left(\frac{n\pi}{L_x}\right)^2} + \left(\frac{n\pi}{L_x}\right)^2 \frac{h}{2}}{\left(\frac{n\pi}{L_x}\right)^2 + \sqrt{k_l^2 - \left(\frac{n\pi}{L_x}\right)^2} \sqrt{k_s^2 - \left(\frac{n\pi}{L_x}\right)^2}}$$

$$C_4(n) = \frac{j \frac{n\pi}{L_x} \left(\frac{jk_s^2}{\sqrt{k_s^2 + k_l^2}} + \left(\frac{k_s^2 k_l^2}{k_s^2 + k_l^2} \right) \frac{h}{2} \right)}{\left(\left(\frac{n\pi}{L_x}\right)^2 - \frac{k_s^2 k_l^2}{k_s^2 + k_l^2} \right) (k_s^2 + k_l^2) \sqrt{\frac{k_s^2 + k_l^2}{k_s^2 k_l^2}}}$$

$$C_5(n) = \frac{j \sqrt{k_l^2 - \left(\frac{n\pi}{L_x}\right)^2} \left(j \sqrt{k_s^2 - \left(\frac{n\pi}{L_x}\right)^2} + \left(\frac{n\pi}{L_x}\right)^2 \frac{h}{2} \right)}{\left(\frac{n\pi}{L_x}\right)^2 + \sqrt{k_l^2 - \left(\frac{n\pi}{L_x}\right)^2} \sqrt{k_s^2 - \left(\frac{n\pi}{L_x}\right)^2}}$$

$$C_6(n) = \frac{-\frac{n\pi}{L_x} \frac{k_l^2}{\sqrt{k_s^2 + k_l^2}} \left(\frac{jk_s^2}{\sqrt{k_s^2 + k_l^2}} + \frac{k_s^2 k_l^2}{k_s^2 + k_l^2} \frac{h}{2} \right)}{\left(\left(\frac{n\pi}{L_x}\right)^2 - \frac{k_s^2 k_l^2}{k_s^2 + k_l^2} \right) (k_s^2 + k_l^2) \sqrt{\frac{k_s^2 + k_l^2}{k_s^2 k_l^2}}}$$

$$C_7(n) = \frac{-j \frac{n\pi h}{L_x} \frac{1}{2} \sqrt{k_l^2 - \left(\frac{n\pi}{L_x}\right)^2} - \frac{n\pi}{L_x}}{\left(\frac{n\pi}{L_x}\right)^2 + \sqrt{k_l^2 - \left(\frac{n\pi}{L_x}\right)^2} \sqrt{k_s^2 - \left(\frac{n\pi}{L_x}\right)^2}}$$

$$C_8(n) = \frac{j \frac{n\pi}{L_x} \sqrt{\frac{k_s^2 k_l^2}{k_s^2 + k_l^2}} \left(\frac{jk_l^2}{\sqrt{k_s^2 + k_l^2}} \frac{h}{2} - 1 \right)}{\left(\left(\frac{n\pi}{L_x}\right)^2 - \frac{k_s^2 k_l^2}{k_s^2 + k_l^2} \right) (k_s^2 + k_l^2) \sqrt{\frac{k_s^2 + k_l^2}{k_s^2 k_l^2}}}$$

$$C_9(n) = \frac{\frac{n\pi}{L_x} \sqrt{k_s^2 - \left(\frac{n\pi}{L_x}\right)^2} \left(\frac{h}{2} \sqrt{k_l^2 - \left(\frac{n\pi}{L_x}\right)^2} - j \right)}{\left(\frac{n\pi}{L_x}\right)^2 + \sqrt{k_l^2 - \left(\frac{n\pi}{L_x}\right)^2} \sqrt{k_s^2 - \left(\frac{n\pi}{L_x}\right)^2}}$$

$$C_{10}(n) = \frac{-\frac{k_s^2}{\sqrt{k_s^2 + k_l^2}} \left(\frac{n\pi}{L_x}\right) \sqrt{\frac{k_s^2 k_l^2}{k_s^2 + k_l^2}} \left(\frac{h}{2} \frac{k_l^2}{\sqrt{k_s^2 + k_l^2}} - j \right)}{\left(\left(\frac{n\pi}{L_x}\right)^2 - \frac{k_s^2 k_l^2}{k_s^2 + k_l^2} \right) (k_s^2 + k_l^2) \sqrt{\frac{k_s^2 + k_l^2}{k_s^2 k_l^2}}}$$

Distribution List

MS1413	1114	T.A.Michalske	MS1111	9221	C.C.Ober
			MS1110	9222	R.C.Allen
MS1425	1315	S.J.Martin	MS1110	9222	D.E.Womble
MS1425	1315	G.C.Frye	MS1110	9223	D.Greenberg
MS1425	1315	M.A.Butler	MS1109	9224	A.L.Hale
MS1425	1315	K.W.Schubert	MS1111	9225	G.Heffelfinger
MS1080	1325	P.J.McWhorter	MS0441	9226	R.Leland
MS1080	1325	J.J.Allen	MS0819	9231	J.M.McGlaun
MS1080	1325	J.J.Sniegowski	MS0819	9231	T.G.Trucano
			MS0820	9232	P.Yarrington
MS0521	1567	S.T.Montgomery			
MS0303	2411	M.J.Forrestal	MS0439	9234	D.R.Martinez
MS0303	2411	B.R.Sturgis	MS0439	9234	J.L.Dohner (10)
MS0303	2411	T.L.Warren	MS0439	9234	D.J.Segalman
			MS0439	9234	C.R.Dohrmann
MS1033	6111	D.S.Drumheller	MS0439	9234	C.Fulcher
MS0705	6114	D.F.Aldridge	MS0439	9234	T.Hinnerichs
			MS0439	9234	D.W.Lobitz
MS9042	8741	T.P.Chen	MS0439	9234	D.B.Longcope
MS9042	8745	W.A.Kawahara	MS0439	9234	G.M.Reese
MS0841	9100	P.J.Hommert	MS0865	9735	J.L.Moya
MS0833	9103	J.H.Biffle	MS0557	9741	T.J.Baca
MS0828	9104	R.Thomas	MS0557	9741	P.S.Barney
MS0826	9111	W.Hermina	MS0557	9741	T.L.Paez
MS0834	9112	A.C.Ratzel			
MS0835	9113	T.C.Bickel	MS1003	9611	T.D. Robinett III
MS0827	9114	R.Griffith	MS1003	9611	J.T. Feddema
MS0827	9114	C.C.Wong			
MS0825	9115	W.H.Rutledge	MS9018	8940-2	Central Tech. Files
MS0833	9103	J.H.Biffle	MS0899	4916	Tech. Library (5)
MS0836	9116	C.W.Peterson	MS0619	12690	Review & Approval Desk (2)
MS0443	9117/9118	H.S.Morgan			For DOE/OST I
MS0437	9117/9118	C.Adams			
MS0443	9117/9118	S.N.Burchett			
MS0443	9117/9118	A.F.Fossum			
MS0443	9117/9118	S.W.Key			
MS0437	9117/9118	S.W.Attaway			
MS0437	9117/9118	D.E.Reedy			
MS0321	9200	W. Camp			
MS9202	9202	R.J.Pryor			
MS1111	9221	S.S.Dosanjh			